The Astrophysical Journal, 700:633–641, 2009 July 20 doi:10.1088/0004-637X/700/1/633

GAMMA-RAY BURST LUMINOSITY FUNCTIONS BASED ON A NEWLY DISCOVERED CORRELATION BETWEEN PEAK SPECTRAL ENERGY AND $V/V_{\rm max}$

Maarten Schmidt
California Institute of Technology, Pasadena, CA 91125, USA
Received 2008 January 8; accepted 2009 May 19; published 2009 July 6

ABSTRACT

We have discovered a correlation between the observed peak spectral energy $E_{\rm pk,obs}$ and the Euclidean value of $\langle V/V_{\rm max}\rangle$ of gamma-ray bursts (GRBs). We present the evidence for the correlation in the GUSBAD catalog and use it to derive the luminosity function of GRBs without using any redshifts. The procedure involves dividing GUSBAD GRBs into five spectral classes based on their $E_{\rm pk,obs}$. The overall luminosity function is derived assuming that each of the spectral classes contributes a Gaussian luminosity function. Their central luminosity is derived from the observed Euclidean $\langle V/V_{\rm max}\rangle$. We explore various forms for the GRB rate function GR(z) in predicting redshift distributions of GRBs detected by *Swift*. We find that GR(z) peaks at a higher redshift than the typical star formation history currently favored in the literature. We consider two examples of GR(z) that successfully predict the observed redshift distribution of *Swift* GRBs. With the luminosity functions in hand, we convert the $E_{\rm pk,obs} - V/V_{\rm max}$ correlation into an $E_{\rm pk,obs} - L_{\rm iso}$ correlation and a rest-frame $E_{\rm pk} - L_{\rm iso}$ correlation. By comparing the $E_{\rm pk} - L_{\rm iso}$ correlation with a published correlation based on GRBs with known $E_{\rm pk,obs}$ and redshifts, we discuss the effect of Malmquist bias.

Key words: distance scale – gamma rays: bursts – methods: statistical

1. INTRODUCTION

The gamma-ray burst (GRB) luminosity function plays a central role in the interpretation of the observed source counts and redshift distributions of GRBs detected with different instruments in different energy bands and to different detection limits. Of particular interest are the resulting rates and the variation with redshift, since these must reflect the properties of the GRB progenitors.

Ideally, the luminosity function is derived from a well defined flux-limited sample of GRBs with redshifts. For most GRB surveys, it is not possible to collect such a sample with well defined gamma-ray and optical flux limits. We will discuss the situation for the *Swift* mission in Section 4.

In the absence of usable redshift statistics, most studies of the luminosity function use luminosity criteria, such as variability (Fenimore & Ramirez-Ruiz 2000) and spectral lag (Norris et al. 2000). We have reviewed several luminosity functions resulting from these studies and found that they generally are not compatible with the source counts and the value of $\langle V/V_{\rm max}\rangle$ for GRBs in the BATSE catalog (Schmidt 2004). As long as this is the case, they cannot provide reliable predictions about redshift distributions, etc.

The correlation between the rest-frame spectral peak energy $E_{\rm pk}$ and the isotropic-equivalent radiated energy $E_{\rm iso}$ found by Amati et al. (2002) seemed to be very promising as a luminosity indicator. However, it has been shown (Nakar & Piran 2005; Band & Preece 2005) that for a large fraction of BATSE bursts there is no redshift that satisfies the Amati relation; for further discussion also see Ghirlanda et al. (2005) and Nakar & Piran (2005). According to Li (2007), a redshift degeneracy in the Amati relation makes it impossible to derive redshifts larger than 0.9 with usable accuracy. Using durations and spectral parameters for GRBs detected by *Swift*, Butler et al. (2007) found a $E_{\rm pk} - E_{\rm iso}$ correlation that is inconsistent with the Amati relation at $> 5\sigma$ significance, with double the scatter. Both Lloyd et al. (2000) and Butler et al. (2007) discussed the effect of detector thresholds on the derivation of $E_{\rm pk} - E_{\rm iso}$ correlations. The latter authors argue that all pre-*Swift* $E_{\rm pk} - E_{\rm iso}$ correlations are likely unrelated to the physical properties of GRBs.

In a study of the GRB luminosity function from 82 HETE-2 GRBs (Pélangeon et al. 2008), an Amati-type correlation was used to derive pseudo-redshifts for the 62 GRBs lacking an observed redshift. This study provides information about low-luminosity GRBs and X-ray flashes that are not represented in the BATSE based GUSBAD Catalog.

In the present study, we introduce a new correlation between the peak spectral energy of the observed peak flux $E_{\rm pk,obs}$ and the Euclidean value of $\langle V/V_{\rm max}\rangle$. The correlation was discovered for GRBs in the GUSBAD catalog.[1] Since the Euclidean value of $\langle V/V_{\rm max}\rangle$ is a geometric cosmological distance indicator (Schmidt 2001), the peak luminosity of a subgroup of GRBs with given $E_{\rm pk,obs}$ can be derived without knowing any redshifts. Using the $E_{\rm pk,obs} - V/V_{\rm max}$ correlation is not subject to any of the problems mentioned above for the Amati relation.

The approach in our paper is the following. We use GUSBAD fluxes in the four BATSE DISCLA channels to divide them into five spectral classes based on their $E_{\rm pk,obs}$ values. We assume that the luminosity function of each spectral group is a Gaussian of $\log L$ with a value of $\sigma_{\log L}$ large enough so that the overall sum of the five luminosity functions is reasonably smooth. In addition, we assume that the overall rate density of GRBs varies with redshift as GR(z). The central luminosity $\log L_c$ of each spectral Gaussian is derived by a process of iteration, until the corresponding value of $V/V_{\rm max}$ for the spectral class agrees with that observed.

The procedure allows deriving the overall GRB luminosity function from the GUSBAD catalog without using any redshifts. The main free parameter is the rate function GR(z). To evaluate the predicted luminosity and redshift distributions for various forms of GR(z), we do need a sample with redshifts. We evaluate and use *Swift* detected GRBs with observed redshifts. For the successful luminosity functions, the process yields a

[1] Available at http://www.astro.caltech.edu/~mxs/grb/GUSBAD.

rest-frame E_{pk} value for each of the spectral classes. This leads to $E_{pk,obs} - L_{iso}$ and $E_{pk} - L_{iso}$ correlations entirely based on data in this paper.

The use of V/V_{max} and the derivation of $E_{pk,obs}$ from GRBs in the GUSBAD catalog are discussed in Section 2, as well as the evidence for the $E_{pk,obs} - V/V_{max}$ correlation. The framework for deriving the luminosity function is discussed in Section 3. The status and completeness of *Swift* observations is covered in Section 4. In Section 5, we present two luminosity functions with differing redshift dependence GR(z) and test them on *Swift* redshift and luminosity distributions. The $E_{pk,obs} - L_{iso}$ and $E_{pk} - L_{iso}$ correlations are derived in Section 6. A discussion and summary follows in Section 7.

2. THE $E_{pk,obs}$–V/V_{max} CORRELATION FOR GUSBAD GRBs

2.1. Euclidean Values of V/V_{max}

The GUSBAD catalog (Schmidt 2006) is based on observations with the BATSE LAD detectors which provide output in four energy channels, viz., 20–50 keV (ch 1), 50–100 keV (ch 2), 100–300 keV (ch 3), and > 300 keV (ch 4). The catalog lists peak photon fluxes for channels 2 and 3 together. These were derived assuming a Band spectrum (Band et al. 1993) with $\alpha = -1.0$, $\beta = -2.0$, and $E_0 = 200$ keV. For the present study, we have derived for each GRB peak photon fluxes in each channel based on the two brightest illuminated LAD detectors.

At the outset of this study, it was not clear whether the four channels of the BATSE LAD detectors could be used for low-resolution spectrophotometry. We decided to use only GRBs with a 50–300 keV peak photon flux P exceeding 0.50 ph cm^{-2} s^{-1}, i.e., twice the effective photon flux limit of the GUSBAD catalog. This still leaves a large sample of 1319 GRBs. The Euclidean value of V/V_{max} is simply $V/V_{max} = (P/P_{lim})^{-3/2}$.

The value of $\langle V/V_{max}\rangle$ for uniformly distributed objects having any luminosity function in Euclidean space is 0.5. This value derives from the fact that volumes are $\sim R^3$ and areas $\sim R^2$. This will not apply in non-Euclidean space, so for cosmological objects the Euclidean value of $\langle V/V_{max}\rangle$ will deviate from 0.5, the more so the larger the typical redshift, i.e., it is a cosmological distance indicator.

Concern has been expressed in the literature about the use of V/V_{max} particularly when sample thresholds vary (Band 1992; Petrosian 1993; Hartmann 1993). The problem of varying threshold can be handled if each object has its own value of P_{lim} as in the GUSBAD catalog. In our present study, the adopted constant limit of 0.50 ph cm^{-2} s^{-1} is larger than all individual limits in the catalog.

All well defined samples above a given flux limit are subject to the Eddington effect (Eddington 1913, 1940). Random errors in the fluxes of individual objects if positive may cause them to become part of the sample, or, if negative, to be lost. Since there are generally more objects in the flux distribution below any given flux than above, the net effect will be that positive errors dominate in the sample. The effect on $\langle V/V_{max}\rangle$ will be that for objects with a uniform distribution, the observed value will be larger than 0.5.

We can evaluate the Eddington effect on $\langle V/V_{max}\rangle$ of our sample through simulations. On the average, σ for GUSBAD fluxes of the second brightest illuminated detector is 0.05 ph cm^{-2} s^{-1}. Our adopted limit of 0.5 ph cm^{-2} s^{-1} (for detector 2) corresponds to ∼1.21 ph cm^{-2} s^{-1} for detectors 1 + 2, with σ = 0.071 ph cm^{-2} s^{-1}. Simulations show that in this case the Eddington excess in $\langle V/V_{max}\rangle$ is 0.002, considerably less than the mean errors of $\langle V/V_{max}\rangle$ for the spectral samples discussed below.

Table 1
Spectral Peak Energies

Channel	n[a]	$E_{pk,obs}$ (keV)[a]	n[b]	$E_{pk,obs}$ (keV)[b]
1	24	30	...	...
2	204	70	4	75
3	608	185	99	202
4	483	420[c]	116	417

Notes.
[a] GUSBAD sample.
[b] Kaneko et al. (2006) data.
[c] Value adopted from Kaneko et al. (2006).

2.2. Deriving Peak Energies

Our goal is to derive the peak energy of the νF_ν spectrum. Given the low spectral resolution, we initially derive $I(E_i) = E_i^2 N(E_i)$ for a representative energy E_i in each BATSE channel i, where $N(E_i)$ is the photon flux density, in ph cm^{-2} s^{-1} keV^{-1}. We used the peak photon fluxes to derive the flux densities $N(E_i)$ at E_i = 30, 70, 185, and 420 keV. For channels 1–3, these energies are close to the geometric means of the energy band limits; for channel 4, see below.

An initial estimate of the peak spectral energy is provided by the channel with the largest value of $I(E_i)$. Table 1 shows for each of the four BATSE channels the number of GRBs having the peak at E_i. We can compare our $E_{pk,obs}$ values with those given by Kaneko et al. (2006) for peak fluxes. Their work was based on BATSE LAD data of 350 bright GRBs in the BATSE catalogs. They used several LAD data types and employed a number of spectral shapes beyond the Band spectrum. The Kaneko list has 219 GRBs that are in the GUSBAD catalog. The last column of Table 1 gives the average Kaneko peak energy for the GUSBAD sources in the Kaneko list. We adopt the Kaneko average for channel 4, since there is no well defined upper energy limit to its energy band. Only for channel 3 is a meaningful comparison possible: our result differs by only 10% from the Kaneko average.

The averages of the Euclidean values of V/V_{max} for peak energies in channels 1–4 are 0.44, 0.45, 0.32, and 0.33, respectively. It turns out that the transition from high to low values of $\langle V/V_{max}\rangle$ takes place within channel 3. Since it contains a large number of peak energies, we subdivide those in channel 3 based on whether the ratio of $I(E_4)/I(E_2)$ is (a) less than 0.5, (b) in the range 0.5–1.0, or (c) larger than 1.0. Given that only 24 objects peak in channel 1, we combine channels 1 and 2. We end up with five spectral peak classes sp with $\langle V/V_{max}\rangle$ ranging from ∼0.45 to ∼0.30, see Table 2. The resulting $E_{pk,obs} - V/V_{max}$ correlation is illustrated in Figure 1.

Table 2 also gives the mean values of α_{23}, the photon spectral index derived from BATSE channels 2 and 3, as given in the GUSBAD catalog. The $\alpha_{23} - V/V_{max}$ correlation had been noted before (Schmidt 2001) in a study similar to the present one.

3. DERIVATION OF SOURCE COUNTS FROM THE LUMINOSITY FUNCTION

Since we do not have redshifts for our sample of GUSBAD GRBs, we cannot derive the luminosity function directly. Instead we iterate the luminosity function by trial and error. In each

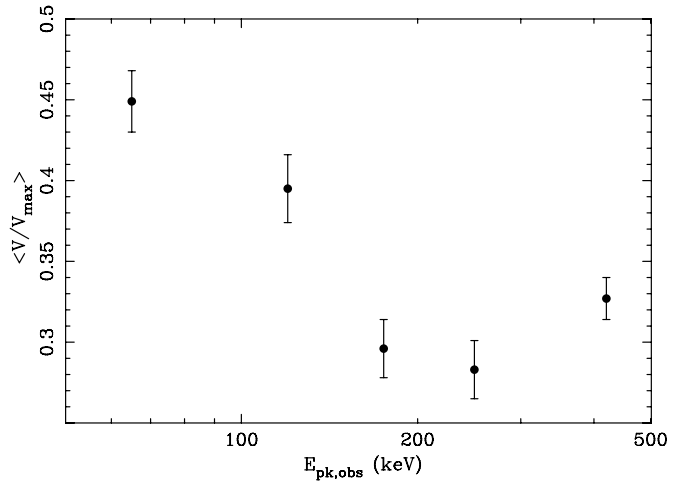

Figure 1. $\langle V/V_{\rm max}\rangle$ values vs. the observed peak spectral energy $E_{\rm pk,obs}$ based on 1319 GUSBAD GRBs with $P > 0.5$ ph cm^{-2} s^{-1}.

Table 2
Peak Spectral Energy, $\langle V/V_{\rm max}\rangle$ and Photon Index

Spectral Classes	Channel	n	$E_{\rm pk,obs}$ (keV)	$\langle V/V_{\rm max}\rangle$	$\langle\alpha_{23}\rangle$
1	1,2	228	65	0.449 ± 0.019	-2.52
2	3[a]	185	120	0.395 ± 0.021	-1.77
3	3[b]	207	175	0.296 ± 0.018	-1.75
4	3[c]	216	250	0.283 ± 0.018	-1.44
5	4	483	420	0.327 ± 0.013	-1.25

Notes.
[a] $I(E_4)/I(E_2) < 0.5$.
[b] $0.5 < I(E_4)/I(E_2) < 1.0$.
[c] $1.0 < I(E_4)/I(E_2)$.

step of the iteration we derive the predicted $\langle V/V_{\rm max}\rangle$ value for each of the spectral classes until they agree with those given in Table 1.

We assume that the GRB luminosity function $\Phi(L, z, {\rm sp})$ of spectral class sp can be written as

$$\Phi(L, z, {\rm sp}) = \Phi_0(L, {\rm sp}){\rm GR}(z), \quad (1)$$

where L is the peak luminosity, $\Phi_0(L, {\rm sp})$ is the $z = 0$ luminosity function of class sp, and GR(z) the comoving GRB rate density, normalized at $z = 0$. We assume that $\Phi_0(L, {\rm sp})$ has a Gaussian distribution

$$\Phi_0(L, {\rm sp}) = \frac{R_0({\rm sp})}{\sigma_{\log L}\sqrt{(2\pi)}} \exp \frac{-[\log L - \log L_c({\rm sp})]^2}{2\sigma^2_{\log L}} \quad (2)$$

with dispersion $\sigma_{\log L}$ around a central peak luminosity L_c(sp). R_0(sp) is the GRB rate at $z = 0$.

Our approach will be to iterate the value of L_c(sp) until the corresponding value of $\langle V/V_{\rm max}\rangle$(sp) for the GUSBAD sample agrees with the observed value. This requires a full derivation of the expected source counts from the luminosity function. The role of $\sigma_{\log L}$ is primarily to make each spectral luminosity function sufficiently wide so that the total luminosity function is reasonably smooth. We ended up using $\sigma_{\log L} = 0.5$.

In deriving fluxes from luminosities and redshifts, we employ the BATSE energy range (E_1, E_2) with $E_1 = 50$ keV and $E_2 = 300$ keV. For an object at redshift z, the observed energy range (E_1, E_2) originates in the range $(E_1(1 + z), E_2(1 + z))$ in the object's rest frame, whereas the luminosity refers to the range (E_1, E_2). The K-term is the ratio of the rest-frame energies radiated in the two ranges,

$$K(z) = \frac{\int_{E1(1+z)}^{E_2(1+z)} EN(E, E_{pk}, \alpha, \beta)dE}{\int_{E_1}^{E_2} EN(E, E_{pk}, \alpha, \beta)dE}. \quad (3)$$

The Band photon spectrum is usually described in terms of a break energy E_0. Here we use a Band spectrum $N(E, E_{pk}, \alpha, \beta)$, where $E_{pk}({\rm sp}) = (2 + \alpha)E_0({\rm sp})$ assuming that $\beta < -2$ (Band et al. 1993). We adopt constant values of $\alpha = -0.8$ and $\beta = -2.6$ for reasons that will be discussed in Section 5.

The peak flux $P(L, z)$ observed for a GRB of luminosity L at redshift z is

$$P(L, z) = \frac{L}{4\pi((c/H_0)A(z))^2} K(z), \quad (4)$$

where $(c/H_0)A(z)$ is the bolometric luminosity distance. We use the cosmological parameters $H_0 = 70$ km s^{-1} Mpc^{-1}, $\Omega_M = 0.3$, and $\Omega_\Lambda = 0.7$.

The integral peak flux distribution for GRBs of spectral class sp is,

$$N(> P, {\rm sp}) = \int \Phi_o(L, {\rm sp})\, dL \int_0^{z(L,\, P,\, sp)} {\rm GR}(z)(1 + z)^{-1}\, (dV(z)/dz)\, dz, \quad (5)$$

where $z(L, P, {\rm sp})$ is derived from Equation (4), $V(z)$ is the comoving volume and the term $(1 + z)^{-1}$ represents the time dilation. With this formulation, it is straightforward to derive the differential source counts $dN(> P, {\rm sp})/dP$, as well as the average values of $V/V_{\rm max}$, $E_{\rm pk,obs}$, α_{23}, etc.

For a given rate function GR(z) the procedure to iterate the luminosity function is as follows. Assume starting values for the central luminosity L_c(sp) and the rest-frame Band peak energy E_{pk}(sp). The differential source counts together with $V/V_{\rm max} = (P/P_{\rm lim})^{-3/2}$ produce the expected values of $\langle V/V_{\rm max}\rangle$(sp) for the GUSBAD catalog. Similarly, the expected values of $E_{\rm pk,obs}$(sp) are obtained by weighting $E_{\rm pk}({\rm sp})/(1 + z)$ with the differential source counts. The iteration is repeated until the expected values of $\langle V/V_{\rm max}\rangle$(sp) and $E_{\rm pk,obs}$(sp) match the observed ones given in Table 2.

It is worth noting that given GR(z) and the shape of the five spectral luminosity functions, the procedure leads for each sp to a single value for L_c(sp) and E_{pk}(sp). The primary unknown is the density function GR(z). We will use *Swift* data to test various forms of GR(z); see Section 5.

4. *Swift* DATA

The *Swift* mission (Gehrels et al. 2004) is in the process of detecting hundreds of GRBs. Thanks to an emphasis on rapid identification and communication, relatively many of these GRBs have observed redshifts. We use this data base to check predicted distributions of redshifts and luminosities based on luminosity functions with different GR(z).

We have used *Swift* GRB data for the period 2005 January 1–2008 September 30. The observations cover a field of view of 1.4 sr in the energy band 15–150 keV. We use observed peak fluxes over a 1 s time interval obtained from the High Energy Astrophysics Science Archive Research Center (HEASARC) and

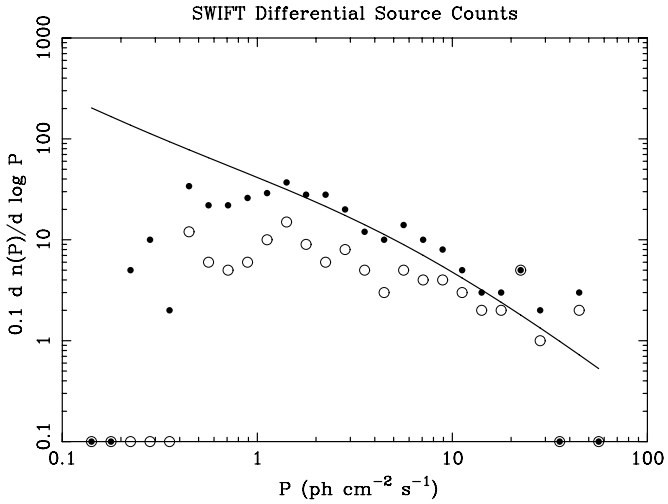

Figure 2. Differential source counts for *Swift*: observed number (dots), those with redshifts (circles), and the predicted number based on a luminosity function (line). Based on this plot, we estimate that the effective completeness limit for *Swift* bursts is $P = 1.0$ ph cm^{-2} s^{-1}.

redshift information from J. Greiner's list.[2] We derive isotropic-equivalent luminosities for the energy band 15–150 keV using the rest-frame $E_{\rm pk} - L_{\rm iso}$ correlation given in Section 6. In deriving these luminosities, we assumed a Malmquist correction $\Delta \log L = +0.36$, see Section 6.

The *Swift* mission does not provide a flux limit above which the sample of GRBs is complete. Band (2006) had analyzed the sensitivity of *Swift* in detail. He concludes that the complexity of the trigger system maximizes the sensitivity, but "makes an accurate determination of this sensitivity at a given time very difficult if not impossible." Given these circumstances, we have to carry out an a posteriori estimate of the effective flux limit above which the burst list is complete.

Following the procedure outlined in Section 3, we can derive the predicted distributions of fluxes, luminosities and redshifts for *Swift*. The predicted flux distribution turns out to be virtually the same for all forms of GR(z) discussed in the following section. We show the distribution in Figure 2, together with the observed number of GRBs and the number of GRBs with observed redshifts. At large fluxes, the prediction appears to be around 9% below the observed numbers. The observed numbers start to deviate systematically below the prediction at $P = 1.0$ ph cm^{-2} s^{-1}. We adopt this flux as the effective completeness limit for the *Swift* bursts. The total number of GRBs above the flux limit is 217, of which 84 have redshifts. The fraction of GRBs with redshifts declines from ~0.6 at large flux to ~0.35 at the limit. We will assume that a redshift fraction of 0.4 applies uniformly above the flux limit.

With the *Swift* flux limit and the fraction with redshifts set, we are now in a position to derive from the luminosity function for a given GR(z) the predicted distributions of luminosity and redshift for the *Swift* sample.

5. EXPLORING LUMINOSITY FUNCTIONS WITH DIFFERENT GR(z) FUNCTIONS

As discussed at the end of Section 3, the only unknown in deriving the GRB luminosity function, given the $E_{\rm pk,obs} - V/V_{\rm max}$ correlation, is the redshift dependence GR(z). Therefore, we can

[2] Available at http://www.mpe.mpg.de/~jcg/grbgen.html.

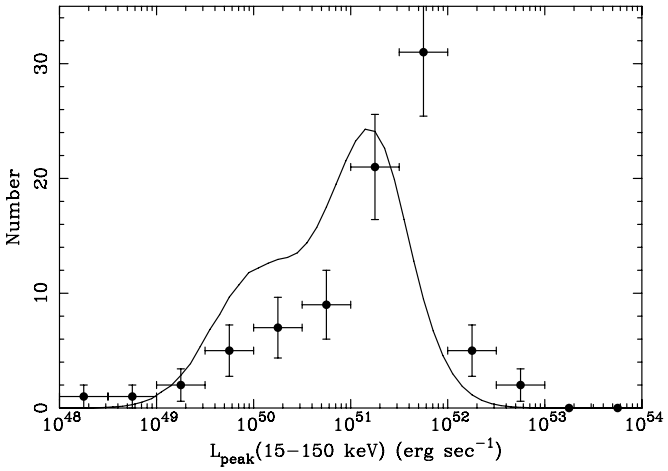

Figure 3. Luminosity distribution of *Swift* sources: observed (dots) and predicted (curve) if GR(z) equals SFH, the typical galaxy star-formation rate, see Equation (6).

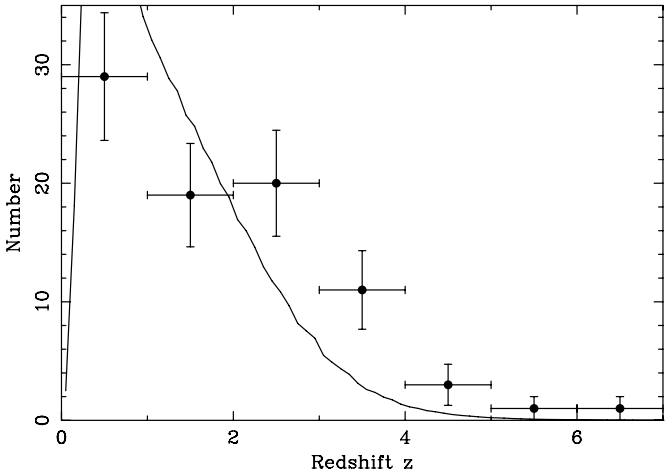

Figure 4. Redshift distribution of *Swift* sources: observed (dots) and predicted (curve) if GR(z) equals SFH, the typical galaxy star-formation rate, see Equation (6).

view the exercise as one in which we explore which shape of GR(z) is compatible with the observations based on *Swift* data.

We first explore the case where GR(z) is the galaxy star formation history (SFH). In the many published studies of star formation in the literature, the SFH rises fast with redshift by about an order of magnitude out to $z \sim 1.5$, beyond which it levels off; it tends to decline beyond $z \sim 3$. We use the analytical expression, normalized to $z = 0$,

$$\rho_{\rm SFH} = (1.0 + (0.10/0.015)z)/(1.0 + (z/3.4)^{5.5}), \qquad (6)$$

for the SFH described by Hopkins & Beacom (2006), based on an extensive compilation by Hopkins (2004).

The predicted distributions of luminosity and redshift are compared to the *Swift* observations in Figures 3 and 4. The predicted number of GRBs (with redshifts) is 79.6, while the observed number is 84. The prediction is ~5% below the observed number. It is obvious that the agreement with the observations is poor, both for the luminosities and the redshifts. We have carried out Monte Carlo simulations to find the probability $P(\log L > 51.5)$ that the observed number of luminosities above $\log L = 51.5$ can be produced from the predicted distribution by chance. We find $P(\log L > 51.5) < 10^{-6}$. Similarly, for redshifts above 3.0 the probability

Table 3
Comparison of Luminosity Function Models

Model	SFH	A	B
GR(z)	$\rho_{\rm SFH}$[a]	$(1+z)^{2.5}$	$(1+z)^{2.0}$
z_c		3.0	4.0
z_d		10.0	10.0
k		0.0	0.0
$P(\log L > 51.5)$[b]	$< 10^{-6}$	0.16	0.18
$P(z > 3.0)$[c]	$< 10^{-6}$	0.93	0.97
$f(z > 2)$[d]	0.198	0.448	0.426
$f(z > 4)$[d]	0.009	0.126	0.159
$f(z > 6)$[d]	0.000	0.037	0.049
$f(z > 8)$[d]	0.000	0.012	0.017

Notes.
[a] Analytical expression for the SFH (Hopkins & Beacom 2006), see Equation (6).
[b] Probability that the model produces the observed number of *Swift* bursts with $\log L > 51.5$.
[c] Probability that the model produces the observed number of *Swift* bursts with $z > 3$.
[d] Fraction of *Swift* bursts with $P > 1.0$ ph cm^{-2} s^{-1} above the given redshift.

$P(z > 3.0) < 10^{-6}$, see Table 3. Even if we continue the SFH beyond the peak redshift $z = 2.55$ at its peak value without any downturn, the agreement remains poor, with $P(\log L > 51.5) < 10^{-6}$ and $P(z > 3.0) = 0.007$. Clearly, the SFH cannot represent GR(z).

With little guidance as to what the shape of GR(z) could be, we use a simple schematic involving a $(1+z)$ power-law rise, a plateau, and an exponential decline with z, as follows:

$$\mathrm{GR}(z) = (1+z)^m, \qquad 0 < z < z_c \tag{7}$$

$$\mathrm{GR}(z) = (1+z_c)^m, \qquad z_c < z < z_d \tag{8}$$

$$\mathrm{GR}(z) = (1+z_c)^m 10^{k(z-z_d)} \qquad z > z_d. \tag{9}$$

With the goal of producing redshift and luminosity distributions more in accord with the observed *Swift* distributions, we explored a number of combinations of the free parameters m and z_c. We concluded from these explorations that to first order the ratio $R = \mathrm{GR}(z=4)/\mathrm{GR}(z=1.5)$ is crucial. This appears related to the fact that most *Swift* bursts have redshifts below 2. For the SFH considered above, the ratio $R = 0.74$.

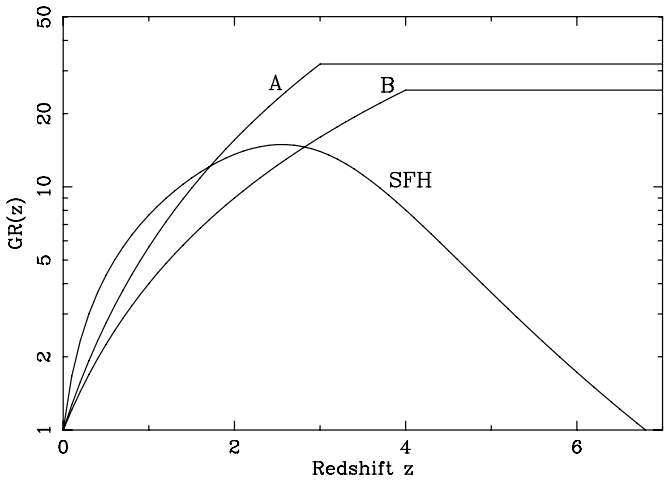

Figure 5. Normalized GRB rates GR(z). The typical star-formation rate SFH produces too few redshifts larger than 2. Models A and B predict luminosity and redshift distributions that are compatible with the *Swift* observations.

We present detailed results for two shapes of GR(z) that have R-values of 3.2 (A) and 4.0 (B), respectively. Table 4 and Figure 5 illustrate the two cases. Case A rises by a factor of 32 to $z = 3.0$ and then remains constant. Case B rises slower to a plateau of 25 starting at $z = 4.0$. We have not actually included the exponential decline beyond z_d. With only two redshifts with $z > 5.0$ in the *Swift* sample, we have no observational leverage on the value of z_d.

The properties of the two models are given in Tables 3 and 4. Both are successful in producing luminosity and redshift distributions compatible with the *Swift* data, see Figures 6 and 7. The redshift distributions predict that 3%–4% of GRBs in the *Swift* sample have $z > 6$ and ~1% $z > 8$. Since we have allowed the density plateau to continue beyond $z = 10$, these percentages are overestimates. Our predictions are lower than most discussed in the literature.

In deriving the luminosity functions, we found that the spectral indices α_{23} given in Table 2 are best represented by the Band spectral parameters $\alpha = -0.8$ and $\beta = -2.6$. We show the observed average spectral index α_{23} for the five spectral classes versus $E_{\rm pk,obs}$ in Figure 8, together with the relation derived from the luminosity functions.

Table 4
Spectral Class Luminosity Functions

Spectral Classes	Case A				Case B			
	$\log L_c$[a]	$\log L_{\rm iso}$[b]	E_0[c]	R_0[d]	$\log L_c$[a]	$\log L_{\rm iso}$[b]	E_0[c]	R_0[d]
1	$49.11^{+0.67}_{-0.57}$	$49.81^{+0.54}_{-0.33}$	73	6.8[e]	$48.93^{+0.45}_{-0.67}$	$49.63^{+0.58}_{-0.47}$	69	13.0[e]
2	$50.84^{+0.27}_{-0.38}$	$51.53^{+0.23}_{-0.33}$	240	0.048	$50.54^{+0.36}_{-0.44}$	$51.14^{+0.31}_{-0.44}$	203	0.149
3	$51.67^{+0.12}_{-0.12}$	$51.97^{+0.06}_{-0.06}$	506	0.0089	$51.71^{+0.13}_{-0.15}$	$52.07^{+0.07}_{-0.07}$	518	0.0133
4	$51.70^{+0.11}_{-0.12}$	$51.95^{+0.06}_{-0.06}$	762	0.0078	$51.75^{+0.12}_{-0.13}$	$52.05^{+0.06}_{-0.06}$	792	0.0112
5	$51.39^{+0.08}_{-0.08}$	$51.76^{+0.04}_{-0.04}$	1217	0.0225	$51.42^{+0.08}_{-0.09}$	$51.85^{+0.04}_{-0.04}$	1244	0.0336

Notes.
[a] Central isotropic-equivalent luminosity of the Gaussian in the 50–300 keV energy band for $\sigma_{\log L} = 0.5$, in erg s^{-1}. Errors correspond to those for $\langle V/V_{\rm max}\rangle$; see Table 2.
[b] Isotropic-equivalent peak luminosity in the 50–300 keV energy band, in erg s^{-1}, see Section 6. Errors correspond to those for $\langle V/V_{\rm max}\rangle$; see Table 2.
[c] Band spectrum break energy in the rest frame, in keV.
[d] GRB density rate at $z = 0$, in Gpc^{-3} yr^{-1}.
[e] Rates for sp = 1 are very uncertain, see Section 5.

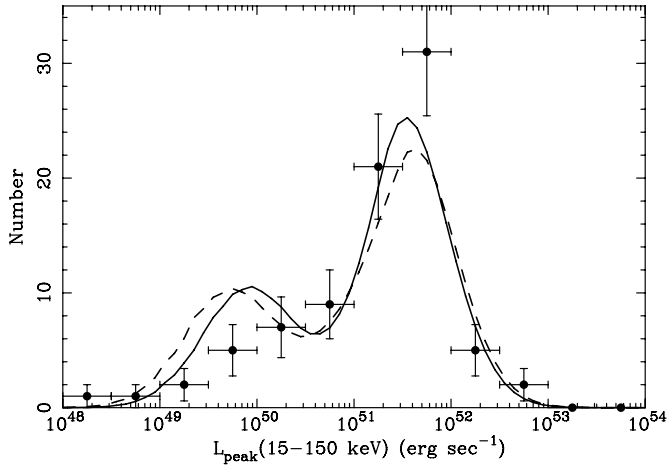

Figure 6. Luminosity distribution of *Swift* sources: observed (dots) and predicted for models A (full line) and B (dashed line).

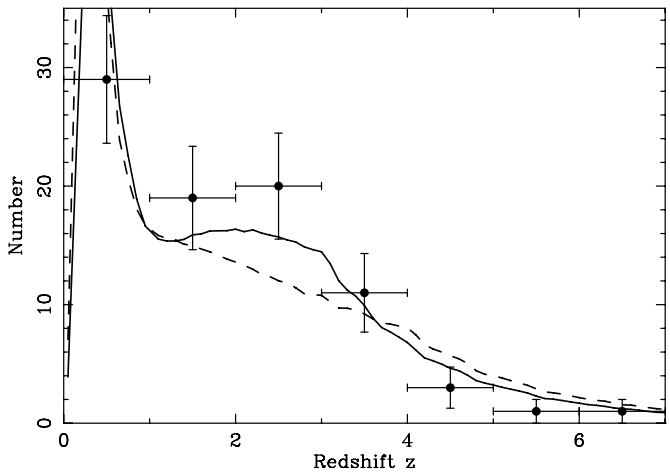

Figure 7. Redshift distribution of *Swift* sources: observed (dots) and predicted for models A (full line) and B (dashed line).

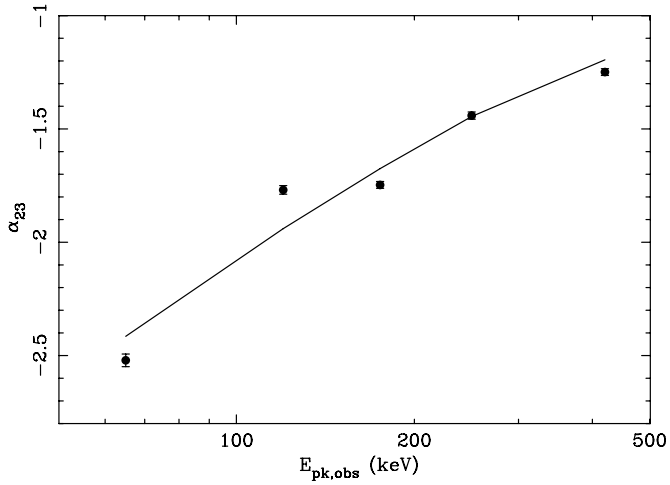

Figure 8. Observed value of the photon index α_{23} vs. the peak spectral energy $E_{\rm pk,obs}$ (points) and average values derived for models A and B (curve) with $\alpha = -0.8$ and $\beta = -2.6$. The error bars for most of the points are too small to show.

We illustrate in Figure 9 the derivation of L_c(sp) from the observed $\langle V/V_{\rm max}\rangle$ values for case A. The differences in the curves reflect the different values of $E_{\rm pk}$ for the spectral classes. For the GUSBAD sample, the curves are only meaningful near

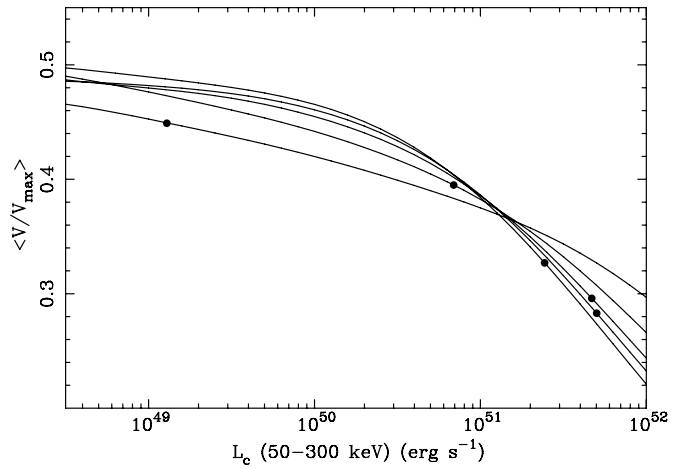

Figure 9. Illustrating the derivation of L_c(sp) from the observed values of $\langle V/V_{\rm max}\rangle$. The points correspond to model A, see Table 4.

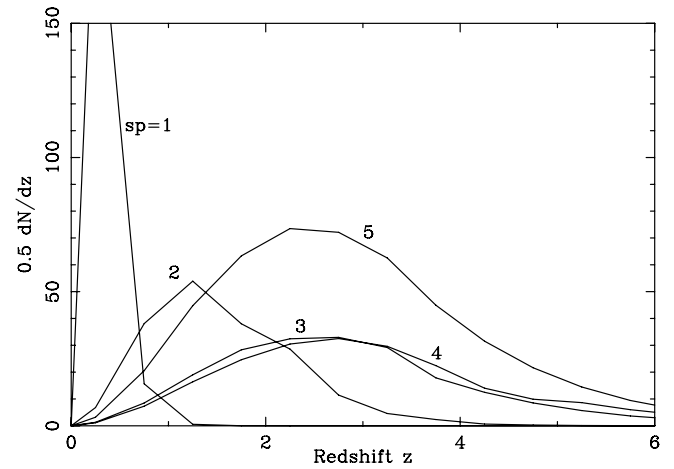

Figure 10. Redshift distribution for the GUSBAD sources, for each of the five spectral classes, based on the luminosity function for model A.

the actual L_c(sp) values. For, say, a deeper sample, the applicable parts would be at correspondingly higher luminosities.

Figure 10 shows the predicted distribution of redshifts for the GUSBAD sample, again based on case A. For sp = 1 essentially all the redshifts are expected to be below 1. This component is very uncertain, as discussed below. The peak redshifts for the different spectral classes reflect their $\langle V/V_{\rm max}\rangle$ values. This illustrates clearly that the Euclidean $\langle V/V_{\rm max}\rangle$ is a cosmological distance indicator.

In Figure 11, we show the luminosity function for case A, as well as the luminosity distribution for the 1319 GUSBAD sources with $P > 0.5$ ph cm^{-2} s^{-1}. Also shown are the individual luminosity functions for the five spectral classes. The first peak of the luminosity function is contributed by spectral class 1. The lower half of its Gaussian clearly plays no role, as it produces no objects in the luminosity distribution. The luminosity assigned to this class is uncertain, since the slope of the curve in Figure 9 is relatively shallow. Actually, if the $\langle V/V_{\rm max}\rangle$ for sp = 1 were only 1.2σ larger, it could not be reproduced by any value of L_c. Altogether, this suggests that the (large) $z = 0$ density rates R_0 for sp = 1 given in Table 4 are very uncertain. The second peak in the luminosity function is contributed by the large number of GRBs in spectral classes 2–5. Their combined $z = 0$ rate is 0.09–0.22 Gpc^{-3} yr^{-1}, for models A and B, respectively.

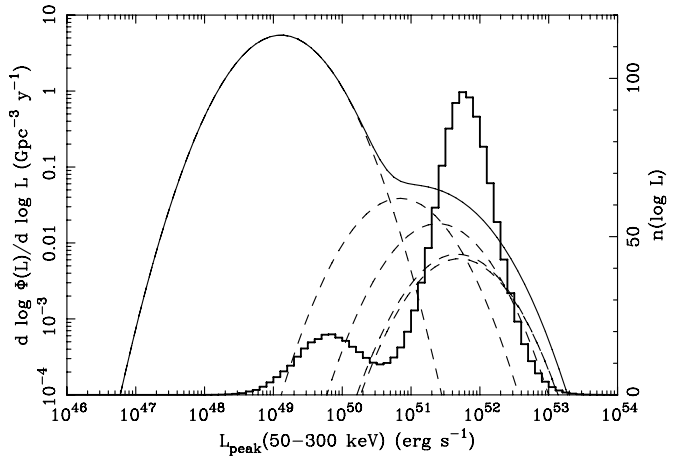

Figure 11. Left side: luminosity function for model A (full line) and the five spectral class luminosity functions (dashed lines). Right side: the corresponding luminosity distribution $n(\log L)$ in steps of $\Delta \log L = 0.1$ for 1319 GUSBAD sources with $P > 0.5$ ph cm^{-2} s^{-1}.

6. THE $E_{pk,obs}-L_{iso}$ AND $E_{pk}-L_{iso}$ CORRELATIONS

E_{pk} correlations with radiated energy or luminosity are of interest in exploring the mechanism for the prompt emission of GRBs. They are also of practical interest in allowing an estimation of the redshift of GRBs with measured $E_{pk,obs}$. In this section, we discuss the derivation of the relevant isotropic-equivalent luminosity L_{iso}, present the $E_{pk,obs} - L_{iso}$ and $E_{pk} - L_{iso}$ correlations, and briefly mention the problem of extracting individual redshifts from E_{pk} correlations.

As discussed in Section 3, the derivation of the luminosity function involves an iteration of the central luminosity L_c(sp), where each spectral component is a Gaussian with dispersion $\sigma_{\log L}$. We chose a dispersion $\sigma_{\log L} = 0.5$ that produces a reasonably smooth overall luminosity function. We want to use the L_c(sp) luminosities in deriving the isotropic-equivalent peak luminosities L_{iso} used in the correlations.

It turns out, however, that L_c(sp) varies considerably with $\sigma_{\log L}$. We explored using $\sigma_{\log L}$ values ranging from 0.1 to 0.6 in deriving the luminosity function for cases A and B. For all values of $\sigma_{\log L}$ the agreement with the observed luminosities and redshifts of the *Swift* GRBs is good. The variation of $\log L_c$(sp) appears to be proportional to $\sigma^2_{\log L}$.

The explanation of the situation is as follows. As $\sigma_{\log L}$ is increased, the wings of the Gaussian will provide more objects with higher and lower luminosities. The higher luminosities will be at larger distances and contribute lower V/V_{max} values. The lower luminosities will contribute higher V/V_{max}, but the shift will be less due to the curvature of the relation between L_c(sp) and V/V_{max}, see Figure 9. The asymmetry results in a higher value of $\langle V/V_{max}\rangle$ requiring a shift to a lower L_c(sp) in order to fit the observed input value of $\langle V/V_{max}\rangle$. The reason why agreement with the *Swift* observations is not affected, is that the additional objects of lower luminosity contribute little to the observed distributions because they are observed over much smaller volumes.

Given our understanding of the variation of L_c(sp) with $\sigma_{\log L}$, it is clear that we want to use the unbiased values of $\log L_c$(sp) at $\sigma_{\log L} = 0$ in deriving the L_{iso}. They are only 0.01–0.03 larger than the $\log L_c$(sp) values for $\sigma_{\log L} = 0.1$. The L_{iso} values given in Table 4 are 2–5 times larger than L_c(sp).

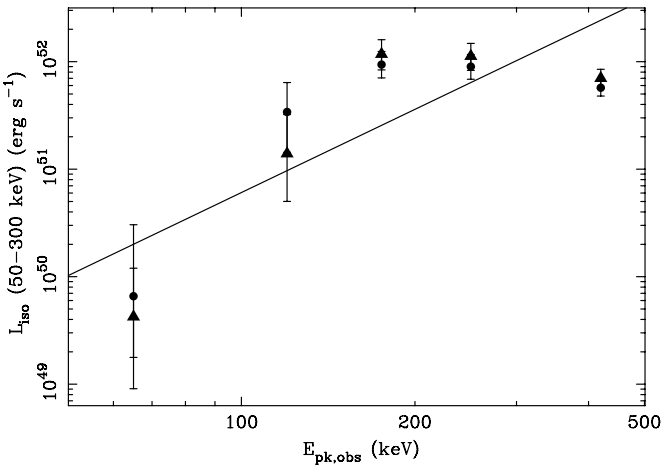

Figure 12. Isotropic-equivalent luminosity L_{iso} vs. the observed $E_{pk,obs}$ for the five spectral classes, for models A (circles) and B (triangles).

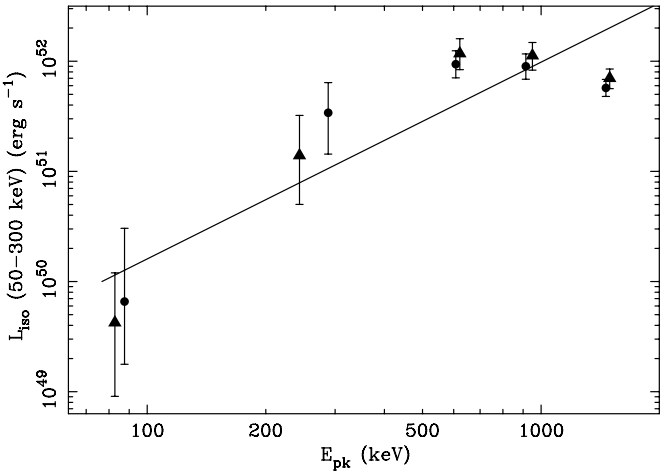

Figure 13. Isotropic-equivalent luminosity L_{iso} vs. the rest-frame E_{pk} for the five spectral classes, for models A (circles) and B (triangles).

We now plot the L_{iso} versus $E_{pk,obs}$ to produce the $E_{pk,obs}-L_{iso}$ correlation in Figure 12. The error bars for L_{iso} reflect the effect of those in $\langle V/V_{max}\rangle$. The line drawn represents a regression of L_{iso} on $E_{pk,obs}$, assuming that the $E_{pk,obs}$ values are errorless,

$$\log L_{iso} = 51.0 + 2.52^{+0.37}_{-0.41}\left(\log E_{pk,obs} - 2.08^{+0.39}_{-0.36}\right). \quad (10)$$

The derivation of the luminosity function involved an iteration not only of the central luminosity L_c(sp), but also of the rest-frame value of the Band peak energy E_{pk}(sp). Figure 13 shows the $E_{pk}-L_{iso}$ correlation. The line drawn represents a regression of L_{iso} on E_{pk},

$$\log L_{iso} = 51.0 + 1.75^{+0.26}_{-0.28}\left(\log E_{pk} - 2.36^{+0.46}_{-0.42}\right). \quad (11)$$

The extraction of individual redshifts from the $E_{pk,obs} - L_{iso}$ correlation for sources with known $E_{pk,obs}$ is straightforward. Using the discrete $E_{pk,obs}$ values of Table 2, we can produce redshifts for all 1319 GRBs without problems. Since the correlation uses the $E_{pk,obs}$ in the observer's frame, it can only be used for GRBs with a 50–300 keV flux larger than 0.5 ph cm^{-2} s^{-1}.

The situation is entirely different for the $E_{pk}-L_{iso}$ correlation. When we use the correlation to derive redshifts for sources with known $E_{pk,obs}$, we find that only 772 out of 1319 GRBs, or

59%, yield a redshift. The situation is strikingly similar to that reported for the Amati relation (Amati et al. 2002) by Nakar & Piran (2005) and Band & Preece (2005), who found that for a large fraction of BATSE bursts there is no redshift that satisfies the relation.

There are relatively few $E_{\rm pk} - L_{\rm iso}$ correlations reported in the literature (Schaefer 2007; Yonetoku et al. 2004). We will compare our correlation with the one given by Schaefer, based on 62 GRBs with $E_{\rm pk,obs}$ values and redshifts,

$$\log L({\rm bol})_{\rm iso} = 52.21 + 1.68(\log E_{\rm pk}/300\,{\rm keV}). \quad (12)$$

Here $\log L$(bol) covers the energy band 1–10,000 keV. Transformation of our 50–300 keV $L_{\rm iso}$ values listed in Table 4 to 1–10,000 keV increases them on the average by 0.61 in $\log L$. Comparison of the bolometric luminosities yields

$$\langle \log L({\rm Schaefer}) - \log L({\rm present})\rangle = +0.52 \pm 0.22. \quad (13)$$

Next we consider the effect of Malmquist bias (Malmquist 1936), the difference in average luminosity of objects observed in a sample above a given flux limit and the average luminosity in space,

$$\Delta \log L = \langle \log L\rangle_{\rm obs} - \langle \log L\rangle_{\rm space}. \quad (14)$$

In Euclidean space, the bias is proportional to $\sigma^2_{\log L}$. For cosmological objects with varying comoving density, the situation is more complex.

All studies of individual GRBs with redshifts aimed at deriving $E_{\rm pk}$ correlations are subject to Malmquist bias since they can only be carried out above some flux limit. The Malmquist bias depends on the luminosity function (in space) of GRBs at given $E_{\rm pk}$. This function is not known at present.

We do have clear evidence of Malmquist bias in the present study. Figure 11 shows that compared to the luminosity functions for the five spectral classes, the luminosity distributions predicted for the GUSBAD sample are shifted to considerably higher luminosities. The Malmquist biases for sp =1–5 are 0.70, 0.53, 0.31, 0.28, and 0.36, respectively, for an average of 0.44. This value is tantalizingly close to the offset shown in Equation (13). However, our values are based on an assumed Gaussian shape of the spectral luminosity functions with a dispersion of $\sigma_{\log L} = 0.5$, designed to make the overall luminosity function reasonably smooth. As long as we do not have reliable information about the distribution of $\log L_{\rm iso}$ at given $E_{\rm pk}$ in space, we will not be able to assess the effect of Malmquist bias accurately.

7. DISCUSSION

We present in this final section some commentary on the approach used in this paper and on the results.

1. This work validates the use of $\langle V/V_{\rm max}\rangle$ as a cosmological distance indicator. It requires a complete sample of GRBs above a well defined flux limit. The GUSBAD catalog with its uniform treatment of all sources is eminently useful for this purpose. The input in the form of $\langle V/V_{\rm max}\rangle$ forced us to a deductive approach where we used a given shape of the (spectral) luminosity function and iterated its center luminosity and rest-frame $E_{\rm pk}$, until the observed $\langle V/V_{\rm max}\rangle$ and $E_{\rm pk,obs}$ were fit. An important advantage of the deductive method is that the derivation of source counts from a given luminosity function can be carried out accurately.
2. This approach is in contrast to the inductive method generally used when redshifts are available. This involves deriving densities in bins of redshift and luminosity and correlating these with redshift and/or luminosity to derive the luminosity function. In such an approach, it is essential to check that the resulting luminosity function produces the input source counts and $\langle V/V_{\rm max}\rangle$ correctly. If this is not the case, predictions about expected numbers of sources at large redshift will be unrealistic (Schmidt 2004).
3. If GRBs were not subject to cosmological evolution, the input in terms of $\langle V/V_{\rm max}\rangle$, $E_{\rm pk,obs}$, and $\langle \alpha_{23}\rangle$ would suffice to derive the luminosity function and hence predict source counts and the redshift and luminosity distributions. Comparing these predictions with the observations, such as from *Swift*, would then constitute a check on the cosmological model. In reality, there is evolution, so in the context of the present study the *Swift* observations of GRBs with redshifts essentially provide information about GR(z).
4. We have indicated that our exploration of various forms for GR(z) indicate that the *Swift* observations seemed to require that the GR($z = 4$)/GR($z = 1.5$) ratio be at least 3. None of the star formation results shown in Figure 1 of Hopkins & Beacom (2006) exhibit such a ratio. Le & Dermer (2006) explored a variety of GRB rate curves and found the best fit for their model SFR6, for which GR($z = 4$)/GR($z = 1.5$) ~ 2. Given that GRBs tend to occur in blue, underluminous galaxies of limited chemical evolution (Fruchter et al. 2006), it is not surprising that GR(z) is different from the main cosmic star formation and concentrated to earlier cosmic times. A study of the hydrogen ionization rate, based on the Lymanα Forest (Faucher-Giguère et al. 2008), concludes that the star formation rate is increasing for $z = 2$–4, qualitatively much like our model B.
5. We have been conservative in setting the effective completeness limit for the *Swift* data at $P = 1.0$ ph cm^{-2} s^{-1} and using only data above the limit. It would be helpful if catalogs of *Swift* sources could include an indication for each source whether it can be considered to be part of a sample that is complete above a given photon limit over a given area.
6. Even while not all individual GRBs can be fitted with a Band spectrum, it appears that for statistical work, the $E_{\rm pk} - L_{\rm iso}$ correlation together with fixed values for $\alpha = -0.8$ and $\beta = -2.6$ provide a surprisingly simple prescription.
7. In comparing $E_{\rm pk} - L_{\rm iso}$ and $E_{\rm pk} - E_{\rm iso}$ correlations, the transformation from the actual energy bands used, like 50–300 or 15–150 keV, to 1–10,000 keV (Amati et al. 2002) introduces needless uncertainty. It would be preferable to report results in the observed energy bands.

This research made use of data obtained from HEASARC, provided by NASA's Goddard Space Flight Center. It is a pleasure to thank Y. Kaneko for detailed information about spectra.

REFERENCES

Amati, L., et al. 2002, A&A, 390, 81
Band, D. L. 1992, ApJ, 400, L63
Band, D. L. 2006, ApJ, 644, 378
Band, D. L., & Preece, R. D. 2005, ApJ, 627, 319
Band, D. L., et al. 1993, ApJ, 413, 281

Butler, N. R., Kocevski, D., Bloom, J. S., & Curtis, J. L. 2007, ApJ, 671, 656
Eddington, A. S. 1913, MNRAS, 73, 359
Eddington, A. S. 1940, MNRAS, 100, 354
Fenimore, E. E., & Ramirez-Ruiz, E. 2000, arXiv:astro-ph/0004176
Fruchter, A. S., et al. 2006, Nature, 441, 463
Faucher-Giguère, C. A., Lidz, A., Hernquist, L., & Zaldarriaga, M. 2008, ApJ, 688, 85
Gehrels, N., et al. 2004, ApJ, 611, 1005
Ghirlanda, G., Ghisellini,, & Firmani, C. 2005, MNRAS, 361, L10
Hartmann, D. H., & The, L.-S. 1993, Ap&SS, 201, 347
Hopkins, A. M. 2004, ApJ, 615, 209
Hopkins, A. M., & Beacom, J. F. 2006, ApJ, 651, 142
Kaneko, Y., Preece, R. D., Briggs, M. S., Paciesas, W. S., Meegan, C. A., & Band, D. L. 2006, ApJS, 166, 298
Le, T., & Dermer, C. D. 2006, ApJ, 661, 394
Li, L. 2007, MNRAS, 374, L20
Lloyd, N. M., Petrosian, V., & Mallozzi, R. S. 2000, ApJ, 534, 227
Malmquist, K. G. 1936, Stockholm Obs. Medd., 26
Nakar, E., & Piran, T. 2005, MNRAS, 360, L73
Norris, J. P., Marani, G., & Bonnell, J. 2000, ApJ, 534, 248
Pélangeon, A., et al. 2008, A&A, 491, 157
Petrosian, V. 1993, ApJ, 402, L33
Schaefer, B. E. 2007, ApJ, 660, 16
Schmidt, M. 2001, ApJ, 552, 36
Schmidt, M. 2004, in ASP Conf. Ser. 312, Third Rome Workshop on Gamma-Ray Bursts in the Afterglow Era, ed. M. Feroci et al. (San Francisco, CA: ASP), 47
Schmidt, M. 2006, ApJ, 616, 1072
Yonetoku, D., Murakami, T., Yamazaki, R., Inoue, A. K., & Ioka, K. 2004, ApJ, 609, 935